The importance of the Voronoi domain partition for position-jump reaction-diffusion processes on non-uniform rectilinear lattices

Christian A. Yates[1,*] and Ruth E. Baker[1,†]

[1] *Centre for Mathematical Biology, Mathematical Institute, University of Oxford, Andrew Wiles Building, Radcliffe Observatory Quarter, Woodstock Road, Oxford, OX2 6GG, UK*

(Dated: October 31, 2013)

PACS numbers: 87.10.-e, 87.10.Ed, 87.10.Mn, 87.10.Hk, 87.16.aj, 82.40.Ck, 87.15.Ya, 87.10.Rt

*yatesc@maths.ox.ac.uk; http://people.maths.ox.ac.uk/yatesc/

†baker@maths.ox.ac.uk; http://people.maths.ox.ac.uk/baker/

I. MORPHOGEN GRADIENT FORMATION EXAMPLE

In this example we consider the formation of a bi-directional morphogen gradient via the addition of molecules to the centre of the domain. We compare two modelling regimes: a stochastic individual-level model and a deterministic population-level partial differential equation (PDE). The individual-based model is a position-jump process on a non-uniform grid as described in the main text. We consider a single molecular species, u, on the domain $[0, 1]$. All molecules in the domain are subject to unimolecular degradation at rate c and diffusion with macroscopic coefficient D. In addition, molecules are added to the central-most interval of the domain at constant rate R. In the individual-based model both reaction and diffusion events are simulated using Gillespie's direct method. Since all reactions are at most first order the deterministic formulation of the model is given by the following PDE

$$\frac{\partial u}{\partial t} = D\frac{\partial^2 u}{\partial x^2} - cu + RH(a, b), \tag{1}$$

with zero-flux boundary conditions at either end. In Eq. (1), $H(a, b)$ is the boxcar step function of unit height which is non-zero on the interval $[a, b]$, where a (b) is the left- (right-) hand end of the interval into which molecules flow in the individual-based model. We initialise the system with $u(x, 0) = 0$ for $x \in [0, 1]$ so that initially the domain is empty of morphogen molecules.

A comparison of the numerical solution of the expected PDE (1) and the mean molecular concentrations averaged over 100 repeats of the individual-based model is given in Fig. 1. The simulations are run for 300 time units, which is sufficient to reach an approximate steady state. We see that the mean molecular concentrations in the individual-based model correspond closely to the concentrations predicted by the PDE.

To quantify the similarity or difference between the PDE solution and the individual-based model we calculate the histogram distance error (HDE) metric [1]. The HDE between two curves (defined at discrete points), having normalized frequencies a_i and b_i at point i (i.e. $\sum a_i = \sum b_i = 1$), is given by

$$HDE = \frac{1}{2}\sum_{i=1}^{k} |a_i - b_i|, \tag{2}$$

where the sum is over all i such that either $a_i \neq 0$ or $b_i \neq 0$.

Close resemblance between the two models over time is further evidenced by the low HDE in Fig. 1 (c). The correspondence between the individual-based model and the PDE in the case of the interval-centred domain is, as expected, poor (data not shown).

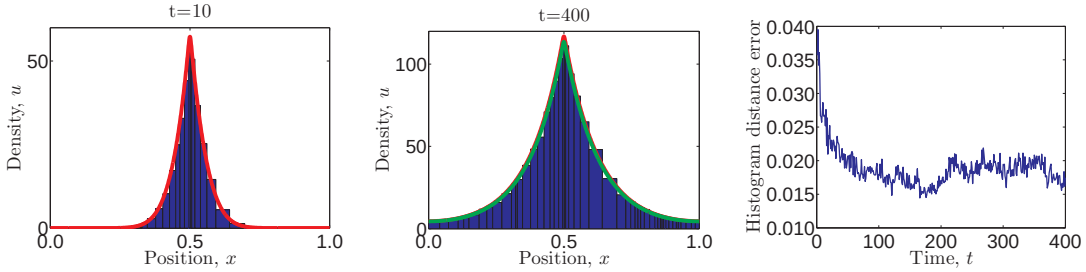

(a) (b) (c)

FIG. 1. *Formation of a bi-directional morphogen gradient. There is a flux of molecules into the central-most interval of the domain and molecules decay at a given rate. In panels (a) and (b) the histograms represent an average over 100 stochastic repeats of the position-jump model with the Voronoi partition. The red curves represent the numerical solution of the PDE* (1) *and the green curve in panel (b) represents the steady state solution of the PDE found analytically. Panel (c) displays the evolution of the HDE between the stochastic simulations and the PDE. The macroscopic diffusion coefficient takes the value* $D = 1/k^2$, *where* $k = 50$. *The other parameter values are* $c = 0.025$ *and* $R = 100$. *The PDE is solved using 1600 grid points and adaptive time-stepping via* `Matlab`*'s one-dimensional PDE solver* `PDEPE`.

II. CONFIRMATORY EXAMPLE OF THE PROPRIETY OF THE VORONOI DOMAIN PARTITION FOR RECTILINEAR LATTICES

Figure 2 displays a snapshot comparison of individual-level and population-level models of diffusion on a rectilinear domain tessellated with rectangles using the Voronoi partition. The molecular concentration profiles in Fig. 2 (a) and (b) (respectively) given by the individual-based and PDE model (respectively) appear similar. Fig. 2 (c) shows a relatively low HDE (*cf* Fig. 3 (c)) indicating that the

individual-level model and the population-level model correspond closely.

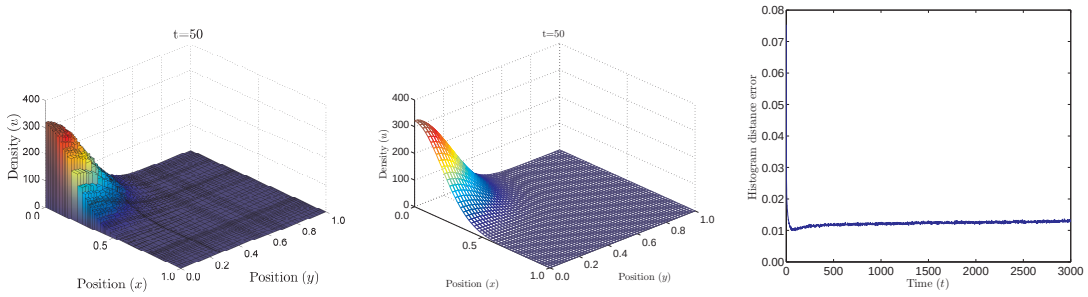

(a) (b) (c)

FIG. 2. *A comparison of the individual-level (with rectilinear domain tessellation) and population-level models of molecules diffusing on the Voronoi domain partition. In the individual-based model the domain is tessellated by 2500 rectangles on a* 50×50 *grid.* $N = 50,000$ *molecules are initialised in the left-most interval of the domain and the PDE initial condition is chosen to replicate this. In both cases zero-flux boundary conditions were implemented on all boundaries in order to conserve molecules. In panel (a) the histograms represent the concentration of molecules in each square of the domain tessellation in the individual-level model. In panel (b) the mesh surface represents the solution of the diffusion equation in two dimensions, with diffusion coefficient* $D = 1/k^2$*, where* $k = 50$*. Panel (c) displays the evolution of the HDE. The initially large value of the HDE is due to the manner in which we are forced to implement the initial condition in the continuum model.*

Conversely Fig. 3 shows a snapshot comparison of individual-level and population-level models of diffusion on a rectilinear grid tessellated using the interval-centred partition. The concentration profiles for the individual-based model (Fig. 3 (a)) and the continuum model (Fig. 3 (b)) no longer appear similar. The strange appearance of the individual-based concentration profile in Fig. 3 (a) is due to the fact that there is no relationship between the rate of molecular flux into and out of a voxel and the area of that voxel in the interval-centred partition. Unlike for the Voronoi partition, this means that large numbers of molecules can be found in voxels with small areas and, as such, the concentration within these voxels can become very large. This is indicated by the consistently large value of the HDE in Fig. 3 (c) which approaches 0.5, the maximum possible value for the HDE (when

the two concentration profiles share the same support).

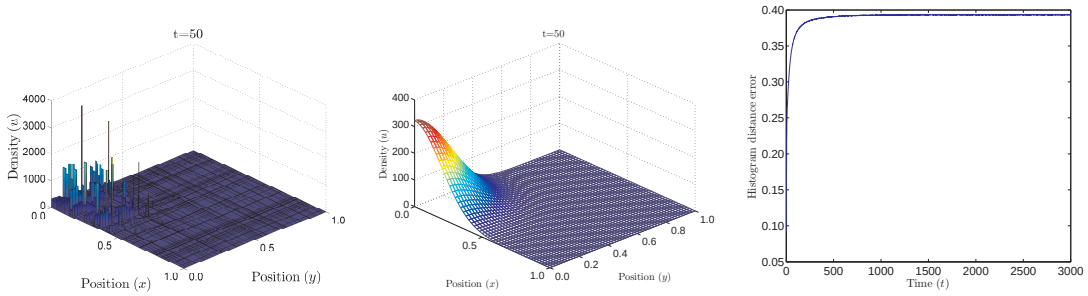

(a) (b) (c)

FIG. 3. *A comparison of the individual-level (with rectilinear domain tessellation) and population-level models of molecules diffusing on the interval-centred domain partition. Figure descriptions, parameters and initial and boundary conditions are as in Fig. 2.*

III. ALTERNATIVE STRUCTURED DOMAIN PARTITIONS

A. Other regular domain partitions

Fig. 4 demonstrates two further domain partitions on which transition rates consistent with the diffusion equation in two dimensions can be derived using Eqs. (6)-(11) of the main text.

For example, on a domain tessellated with equilateral triangles with sides of length h (Fig. 4 (a)). In order to recapitulate the diffusion equation the transition rates should be

$$T_{l_0}^{l_j} = T_{l_j}^{l_0} = \frac{4D}{h^2}, \qquad \text{for} \qquad j = 1, 2, 3. \tag{3}$$

Similarly, if we tessellate the domain with hexagons of side h (Fig. 4 (b)) we can choose transition rates

$$T_{l_0}^{l_j} = T_{l_j}^{l_0} = \frac{2D}{9h^2}, \qquad \text{for} \qquad j = 1, \ldots, 6, \tag{4}$$

in order to regain the diffusion equation in the continuum limit.

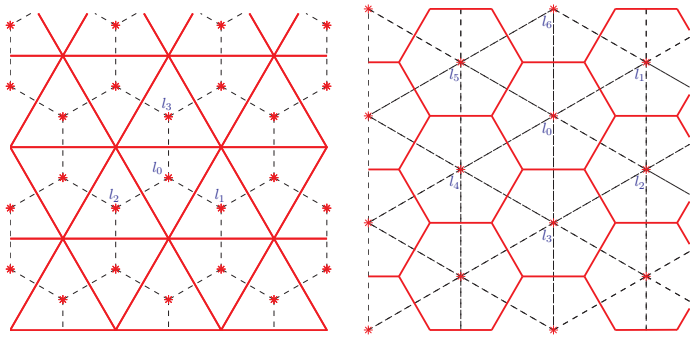

(a) (b)

FIG. 4. *(a) Triangular and (b) hexagonal domain tessellations. Voxel boundaries are demarcated in red. The grid on which the molecules move is displayed using a dashed black line and the points at which the molecules reside in each element are represented by red stars (*).*

B. Semi-regular domain partitions

There are also domain tessellations which allow the derivation of consistent transition rates which are not Voronoi tessellations. Consider the semi-regular octagon-square tessellation (Fig. 5 (a)). Assuming both the squares and the octagons have sides of length h then the distance between the centre of a square and the centre of a neighbouring octagon is $\Delta x_{so} = h(1+\sqrt{2})$ and the distance between the centres of two neighbouring octagons is $\Delta x_{oo} = h(2+\sqrt{2})$. As before, employing Eqs. (6)-(11) of the main text for the square-centred stencil and the octagon-centred stencil sequentially we can derive transition rates which correspond to the diffusion equation in the continuum limit:

$$T_s^o = \frac{D}{h^2(1+\sqrt{2})^2}, \tag{5}$$

$$T_o^s = \frac{DA_s}{A_o h^2(1+\sqrt{2})^2}, \tag{6}$$

$$T_o^o = \frac{D}{2h^2(1+\sqrt{2})^2}\left(1-\frac{A_s}{A_o}\right), \tag{7}$$

where $A_s = h^2$ represents the area of the square and $A_o = 2h^2(1+\sqrt{2})$ the area of the octagon. T_s^o represents the transition rate from the square to the octagon, T_o^s from octagon to square and T_o^o from octagon to octagon [2].

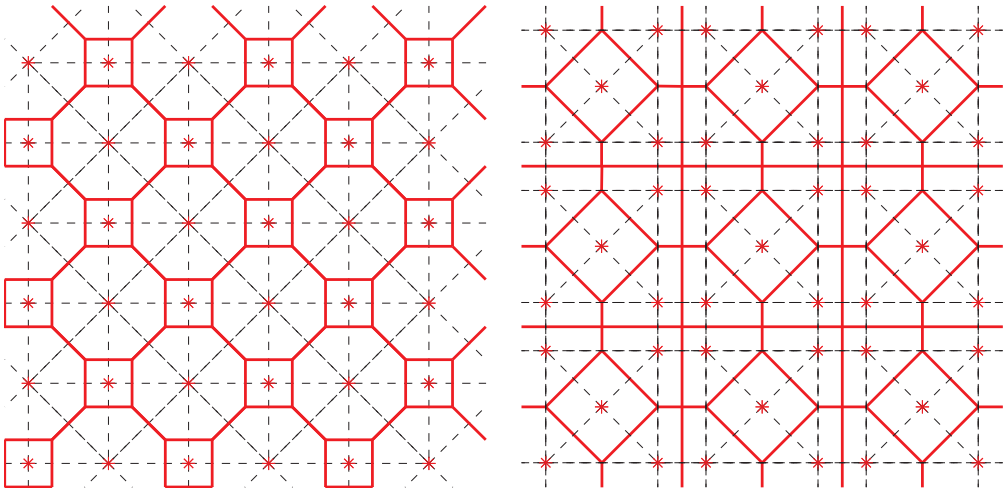

(a) (b)

FIG. 5. *(a) Octagon-square and (b) square-pentagon domain tessellations. Figure descriptions are as in Fig. 4.*

Clearly the octagon-square tessellation is not Voronoi since the underlying grid points are on a square lattice and the Voronoi tessellation corresponding to a square lattice is a square tessellation. The symmetry of the lattice allows us to trivially satisfy Eqs. (7), (8) and (10) for each stencil without specifying anything about the transition rates. Equations (9) and (11) collapse onto one equation for each of the two stencils also due to symmetry and Eq. (6) gives the same relationship for each stencil. This leaves us with three equations for the three unknown transition rates. In this situation the symmetry of the situation allowed us to satisfy the necessary equations, however, in general for a non-uniform lattice this will not be the case.

Conversely there are Voronoi partitions which do not support the derivation of transition rates consistent with a macroscale representation of diffusion. For example, consider the centroidal Voronoi tessellation of squares and pentagons given in Fig. 5 (b). There are four transition rates to be determined representing the four possible movements between neighbouring intervals. After allowing for symmetry and redundancy in the equations, we are left with five equations to solve. In particular, when considering the pentagon-centred scheme we find that in order to satisfy Eq. (10) we must choose $T_s^p = 0$ (the transition rate from squares to pentagons).

This contradicts the value of T_s^p found by considering the square-centred partition.

---

[1] Y. Cao and L. Petzold. Accuracy limitations and the measurement of errors in the stochastic simulation of chemically reacting systems. *J. Comput. Phys.*, 212(1):6–24, 2005.

[2] There is no square to square transition rate, T_s^s, since squares are not adjacent to each other in the octagon-square tessellation.